Online Estimation and Coverage Control with Heterogeneous Sensing Information

Andrew McDonald Lai Wei Vaibhav Srivastava

***Abstract*— Heterogeneous multi-robot sensing systems are often able to characterize physical processes—such as pollution events or wildfires—more comprehensively than homogeneous systems. Access to multiple modalities of sensory data allows heterogeneous systems to fuse information from different sources and ultimately learn a richer representation of the process of interest. These data typically consist of multiple correlated levels of fidelity ranging in accuracy (bias) and precision (noise). Low-fidelity data may be more plentiful, while high-fidelity data may be more trustworthy. In this paper, we draw inspiration from techniques originating in the field of multi-fidelity modeling and apply them to the problem of multi-robot online estimation and coverage control, using a combination of low- and high-fidelity data to learn and cover a sensory function of interest. Specifically, we leverage multi-fidelity Gaussian Process regression to (i) fuse heterogeneous sensory data and learn an unknown sensory function while (ii) simultaneously performing coverage on the inferred function. We propose two algorithms for this task of heterogeneous learning and coverage—namely Stochastic-sequencing of Multi-fidelity Learning and Coverage (SMLC) and Deterministic-sequencing of Multi-fidelity Learning and Coverage (DMLC)—and prove they converge asymptotically. In addition, we demonstrate the empirical efficacy of SMLC and DMLC through numerical simulations.**

I. Introduction

Heterogeneous multi-robot sensing systems—in which agents measure a phenomenon of interest through multiple distinct modalities—often outperform homogeneous systems, in which agents are limited to a single sensory modality. By fusing information across modalities, heterogeneous multi-robot sensing systems are able to learn a more accurate representation of the phenomenon of interest. For example, a network of drones and unmanned aquatic vehicles monitoring the waters of a lake or ocean may together be able to detect harmful algal blooms (HABs) [1] more accurately than a homogeneous system consisting exclusively of one or the other. Computational analysis of drone imagery combined with *in-situ* measurements of chemical concentrations by unmanned aquatic vehicles offer a more comprehensive view than that from a single data source: the geographic extent of a HAB may be easier to detect from the characteristic large green patches visible in drone imagery, while the precise levels of cyanotoxins may be easier to detect through direct analysis of water samples (Figure 1). In spite of this promise, however, heterogeneous multi-robot sensing systems give rise to a new class of challenges which do not emerge in homogeneous systems. The goal of this paper is to address such challenges associated with the tasks of inference and coverage in heterogeneous multi-robot sensing systems.

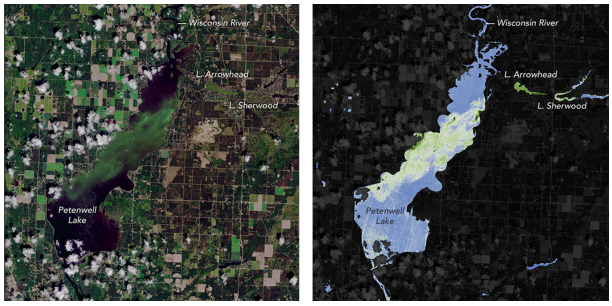

Fig. 1: Satellite imagery (left) and concentration of chlorophyll-a (right) indicative of a harmful algal bloom (HAB) in Petenwell Lake, WI, USA.[1] A heterogeneous multi-robot sensing system with drones and aquatic agents combining data from imagery and chemical samples may be able to detect such HABs more accurately than homogeneous systems limited to one type of data.

Agents performing *coverage* [2] aim to distribute themselves over a region and collectively measure a phenomenon of interest as accurately as possible. Originally formulated under the assumption that agents are homogeneous and have perfect knowledge of the phenomenon of interest, a number of works have considered the extension of coverage to heterogeneous sensing systems [3]–[8]. The class of heterogeneity considered in these works include differences in sensing and actuation footprints [4]–[7], as well as heterogeneity of sensory functions to be covered [8].

However, these works maintain the assumption that the density function ϕ describing the phenomenon of interest is known, when in practice ϕ is often unknown *a priori*. On the other hand, [9]–[16] consider homogeneous agents and forego the assumption that ϕ is known, allowing ϕ to be learned from data to perform *online estimation and coverage*. In particular, [11] presents stochastic online estimation and coverage algorithms with convergence guarantees which inspire this work, and [16] presents a deterministic approach which we extend in this paper. Yet aside from a brief mention in [17], the problem of of online estimation and coverage with heterogeneous agents remains an open area of research.

In this paper, we consider online estimation and coverage

This work has been supported in part by NSF grant IIS-1734272 and ARO grant W911NF-18-1-0325.

A. McDonald is with the Department of Computer Science and Engineering. Michigan State University, East Lansing, MI 48823 USA. e-mail: mcdon499@msu.edu

L. Wei and V. Srivastava are with the Department of Electrical and Computer Engineering. Michigan State University, East Lansing, MI 48823 USA. e-mail: {weilai1, vaibhav}@msu.edu

[1]Courtesy of NASA Earth Observatory/Joshua Stevens via https://www.nasa.gov/feature/goddard/2019/nasa-helps-warn-of-harmful-algal-blooms-clouding-lakes-reservoirs.

in robotic systems in which data of multiple modalities (fidelities) is available. That is, we assume agents with heterogeneous sensing capabilities collect data pertaining to the same physical process of interest with density ϕ, where high-fidelity data provides an accurate representation of the process and low-fidelity data provides a noisy, biased representation of the process. Nonetheless, we assume low-fidelity data is positively correlated to high-fidelity data such that it provides meaningful insight into the true physical process described by ϕ.

Examples of such heterogeneous sensing include scenarios in which an estimate of the phenomenon of interest is available from satellite or aerial imagery data, or the estimates are provided by a human. The sensing data from satellites or aerial imagery is indeed low resolution compared with high-fidelity sensing data obtained by on-ground robots in real time. Likewise, experiments with humans [18] have shown that their input captures the structure of the environment in terms of spatial correlations but can be biased. The heterogeneous sensing could also be an outcome of sensor scheduling on homogeneous robots to handle sensing trade-offs [19] or energy constraints [20].

We present a principled approach to jointly learning and covering ϕ given data at multiple fidelities. The main contributions of this work include two online multi-fidelity estimation and coverage algorithms—namely Stochastic-sequencing of Multi-fidelity Learning and Coverage (SMLC) and Deterministic-sequencing of Multi-fidelity Learning and Coverage (DMLC)—along with an asymptotic analysis of their convergence and numerical illustrations of their efficacy.

The remainder of the paper is organized as follows. Section II formulates the online estimation and coverage problem and describes the approach used to model heterogeneous sensing information. Section III then presents SMLC and DMLC, and proves their asymptotic convergence. Section IV compares the performance of SMLC and DMLC with single-fidelity approaches, presenting numerical results which illustrate the empirical success of the multi-fidelity approach. Finally, Section V summarizes the key contributions of our work and provides concluding remarks.

II. Problem Formulation & Preliminaries

In this section, we present the online estimation and coverage problem in the presence of heterogeneous sensing information. We first recall the coverage problem and describe the model of heterogeneous sensing information considered in this paper. We then combine these ideas to formulate the online estimation and coverage problem.

A. Coverage Problem and Lloyd's Algorithm

Consider the operation of N mobile sensing agents indexed by $i \in \{1, 2, \dots, N\}$ in a compact, convex 2D environment $\mathcal{D} \subset \mathbb{R}^2$. Suppose there exists a sensory function $\phi : \mathcal{D} \to \mathbb{R}_{\geq 0}$ that measures some quantity of interest $\phi(\boldsymbol{x})$ at each point $\boldsymbol{x} \in \mathcal{D}$. Intuitively, ϕ can be interpreted as the importance of each $\boldsymbol{x} \in \mathcal{D}$, such that $\phi(\boldsymbol{x}) > \phi(\boldsymbol{x}')$ encodes the fact that more sensing is needed at $\boldsymbol{x}$ than $\boldsymbol{x}'$. The N agents are distributed across $\mathcal{D}$ to form a configuration $\boldsymbol{\eta} \in \mathcal{D}^N$, wherein the i-th element corresponds to the location of agent i. Let $P = \{p_i\}_{i=1}^N$ be an N-partition of $\mathcal{D}$. Assigning each region p_i to the i-th agent, the *coverage loss* $\mathcal{L}_\phi(\boldsymbol{\eta}, P)$ corresponding to configuration $\boldsymbol{\eta}$, N-partition P and sensory function ϕ is defined to be

$$\mathcal{L}_\phi(\boldsymbol{\eta}, P) = \sum_{i=1}^{N} \int_{p_i} \|\boldsymbol{q} - \boldsymbol{x}_i\|^2 \phi(\boldsymbol{q}) d\boldsymbol{q}, \tag{1}$$

where $\|\cdot\|$ denotes the standard Euclidean norm in $\mathbb{R}^2$. The objective is to reach a configuration-partition pair $(\boldsymbol{\eta}, P)$ that minimizes $\mathcal{L}_\phi(\boldsymbol{\eta}, P)$.

For a given configuration $\boldsymbol{\eta}$, the loss function (1) is minimized by the so called Voronoi partition $\mathcal{V}_\mathcal{D}(\boldsymbol{\eta}) = \{v_i\}_{i=1}^N$ with each partition v_i defined by

$$v_i = \left\{ \boldsymbol{q} \in \mathcal{D} \mid \|\boldsymbol{q} - \boldsymbol{\eta}_i\| < \|\boldsymbol{q} - \boldsymbol{\eta}_j\| \quad \forall\, j \neq i \right\}. \tag{2}$$

Likewise, for a given partition P, the loss function (1) is minimized by configuration $\boldsymbol{c}(P) = (\boldsymbol{c}_1(p_1), \dots, \boldsymbol{c}_N(p_N))$, where each $\boldsymbol{c}_i(p_i)$ is the *centroid* of $p_i \in P$ defined by

$$\boldsymbol{c}_i(p_i) = \frac{1}{m_i(p_i)} \int_{p_i} \boldsymbol{q}\phi(\boldsymbol{q}) d\boldsymbol{q}, \; m_i(p_i) = \int_{p_i} \phi(\boldsymbol{q}) d\boldsymbol{q}. \tag{3}$$

A Voronoi partition $\mathcal{V}_\mathcal{D}(\boldsymbol{\eta}^*)$ is called a *centroidal Voronoi partition* if $\boldsymbol{\eta}^* = \boldsymbol{c}(\mathcal{V}_\mathcal{D}(\boldsymbol{\eta}^*))$. In general, it is hard to find the global minimum of (1) due to the nonconvexity of $\mathcal{L}_\phi(\boldsymbol{\eta}, P)$. However, a configuration corresponding to a centroidal Voronoi partition is considered to be an efficient solution to the coverage problem [2]. To achieve such a partition, one may iteratively apply Lloyd's algorithm [21] initialized from an arbitrary starting configuration $\boldsymbol{\eta}^{(0)}$ using

$$\boldsymbol{\eta}^{(t+1)} = \left(\boldsymbol{c}_1(\mathcal{V}_\mathcal{D}(\boldsymbol{\eta}^{(t)})), \dots, \boldsymbol{c}_N(\mathcal{V}_\mathcal{D}(\boldsymbol{\eta}^{(t)})) \right). \tag{4}$$

It is known that $\mathcal{V}_\mathcal{D}(\boldsymbol{\eta}^{(t)})$ converges to a centroidal Voronoi partition as $t \to \infty$.

B. Modeling Heterogeneous Sensing Data as MFGP

To motivate the idea, suppose a team of robots are deployed to a polluted area within a lake or ocean. To efficiently prevent further spread of pollution, it is important to know the concentration of pollutant over the area of interest, represented by the sensory function ϕ. In this task, multiple sources of sensing information can be used: for example, satellite imagery, drone observations, as well as chemical concentrations collected by aquatic agents. The fidelity level of sensory data varies among different sources.

Suppose there are a total of s types of sensing sources, each of which is indexed by fidelity level $f = \{1, \dots, s\}$. The sensory function at each fidelity level $f < s$ denoted by $\phi_f : \mathcal{D} \to \mathbb{R}_{\geq 0}$ can be viewed as an approximation of ϕ and we assume $\phi_s = \phi$ is the ground truth. We model $\phi_1, \dots, \phi_s$ as a Multi-Fidelity Gaussian Process (MFGP) [22] in which

$$\phi_f = \rho_{f-1}\phi_{f-1} + \delta_f \quad \forall f \in \{2, \dots, s\}, \tag{5}$$

where $\rho_{f-1} > 0$ is a scaling factor, $\phi_1 = \delta_1$, and $\delta_f \sim GP(\mu^f(\boldsymbol{x}), k^f(\boldsymbol{x}, \boldsymbol{x}'))$, $f \in \{1, \dots, s\}$ are mutually

independent GPs. With this structure, δ_f refines the information from lower fidelity to compose the higher fidelity information.

At each fidelity f, ϕ_f can be accessed by taking a sample at $\boldsymbol{x} \in \mathcal{D}$ to obtain a measurement of form $y_f = \phi_f(\boldsymbol{x}) + \varepsilon_f$ where $\varepsilon_f \sim \mathcal{N}(0, \sigma_f^2)$ is additive noise. Let the number of measurements at fidelity f be n_f and $X_f \in \mathbb{R}^{2\times n_f}$ be the matrix of sampling locations. Let these n_f measurements be collected in vector $\boldsymbol{y}_f \in \mathbb{R}^{n_f}$. We now recall the posterior distribution of ϕ from [19].

Let $K^i\big(X_f, X_{f'}\big) \in \mathbb{R}^{n_f \times n'_f}$ be a matrix with entries $k^i(\boldsymbol{x}, \boldsymbol{x}')$, $\boldsymbol{x} \in \text{col}\,\big(X_f\big)$, $\boldsymbol{x}' \in \text{col}\,\big(X_{f'}\big)$ and $K^i(X_f, \boldsymbol{x}) \in \mathbb{R}^{n_f}$ be a vector with entries $k^i(\boldsymbol{x}', \boldsymbol{x}), \boldsymbol{x}' \in \text{col}\,\big(X_f\big)$. We define $\rho_{f:f'} = \prod_{i=f}^{f'-1} \rho_i$ if $f < f'$ and $\rho_{f:f'} = 1$ if $f = f'$. Let $\boldsymbol{K}$ be an $s \times s$ block matrix with $\big(f, f'\big)$ submatrix being the covariance matrix of $\boldsymbol{y}_f$ and $\boldsymbol{y}'_f$ expressed as

$$\boldsymbol{K}_{f,f'} = \sum_{i=1}^{\min(f,f')} \rho_{i:f}\rho_{i:f'} K^i\big(X_f, X_{f'}\big).$$

Let $\boldsymbol{k}(\boldsymbol{x})$ be a vector constructed by concatenating s subvectors $\boldsymbol{k}(\boldsymbol{x}) = \big(\boldsymbol{k}^1(\boldsymbol{x}), \ldots, \boldsymbol{k}^s(\boldsymbol{x})\big)$, where

$$\boldsymbol{k}^f(\boldsymbol{x}) = \sum_{i=1}^{f} \rho_{i:f}\rho_{i:s} K^i(P_n^f, \boldsymbol{x}), \quad \forall f \in \{1, \ldots, s\}.$$

We denote the $s \times s$ diagonal matrix with variance of sampling noise at diagonal entries by $\boldsymbol{\Theta}$:

$$\boldsymbol{\Theta} = \text{diag}\left\{\sigma_f^2 I_{n_f}\right\}_{f=\{1,\ldots,s\}}.$$

Let $\mu^i(X_f) \in \mathbb{R}^{n_f}$ be a vector with entries $\mu^i(\boldsymbol{x})$, $\boldsymbol{x} \in \text{col}\,\big(X_f\big)$. Let the mean of $\boldsymbol{y}_f$ be $\boldsymbol{m}_f = \sum_{i=1}^{f} \rho_{i:f}\mu^i(X_f)$. Construct $\boldsymbol{\nu}$ by concatenating s subvectors, $\boldsymbol{\nu} = (\boldsymbol{y}_1 - \boldsymbol{m}_1, \ldots, \boldsymbol{y}_s - \boldsymbol{m}_s)$. Then, the posterior mean and covariance functions of ϕ are

$$\mu'(\boldsymbol{x}) = \mu(\boldsymbol{x}) + \boldsymbol{k}^\top(\boldsymbol{x})\left(\boldsymbol{K} + \boldsymbol{\Theta}\right)^{-1}\boldsymbol{\nu} \tag{6}$$

$$k'\left(\boldsymbol{x}, \boldsymbol{x}'\right) = k\left(\boldsymbol{x}, \boldsymbol{x}'\right) - \boldsymbol{k}^\top(\boldsymbol{x})\left(\boldsymbol{K} + \boldsymbol{\Theta}\right)^{-1}\boldsymbol{k}(\boldsymbol{x}'), \tag{7}$$

where $\mu(\boldsymbol{x})$ and $k(\boldsymbol{x}, \boldsymbol{x}')$ are the prior mean function and covariance function of ϕ with expression

$$\mu(\boldsymbol{x}) = \sum_{i=1}^{s} \rho_{i:s}\mu^i(\boldsymbol{x}),\ k(\boldsymbol{x}, \boldsymbol{x}') = \sum_{i=1}^{s} \rho_{i:s}^2 k^i(\boldsymbol{x}, \boldsymbol{x}'). \tag{8}$$

C. Online Coverage with Heterogeneous Sensing Data

In the online coverage problem, ϕ is unknown *a priori* and must be learned from heterogeneous sensing data. The proposed framework handles two classes of sensing heterogeneity: (i) heterogeneity due to different sensing sources, such as satellite, aerial vehicle, and human input, that are available at the beginning and are used to efficiently initialize the algorithm, and (ii) heterogeneity introduced due to sensing modality chosen by the robot in order to expedite learning, which appears during the execution of the algorithm. For simplicity of exposition, we focus on the first class of heterogeneity in the remaining paper. Additionally, we will restrict the presentation to two fidelity levels: low (ℓ) and high (h). The low-fidelity sensing data may correspond to sources in (i), and the high-fidelity sensing data may correspond to the real time measurements obtained by robots. However, the ideas presented extend to the second class of heterogeneity and more than two levels of fidelities.

We assume the data from all sources are gathered at an information center (e.g., a cloud) and can be transferred to any functional agent instantaneously, which means each agent is able to compute the same posterior distribution of ϕ. While completing the task, the agents keep collecting information about ϕ and update their estimate of ϕ and coverage strategy. Because the task of sensing could lead agents to deviate from providing coverage service, learning must be carefully scheduled to maintain a satisfactory overall coverage performance. Hence, we evaluate the coverage performance by evaluating the deviation from the set of centroidal Voronoi partitions. Accordingly, for the robot-team configuration $\boldsymbol{\eta}^{(t)}$ at time t, the *instantaneous coverage regret* is defined as

$$R_\phi^{(t)} = \mathcal{L}_\phi\left(\boldsymbol{\eta}^{(t)}, \boldsymbol{c}\big(\mathcal{V}_\mathcal{D}(\boldsymbol{\eta}^{(t)})\big)\right) - \mathcal{L}_\phi\left(\boldsymbol{\eta}^{(t)}, \mathcal{V}_\mathcal{D}(\boldsymbol{\eta}^{(t)})\right), \tag{9}$$

which is nonnegative and achieves 0 at a centroidal Voronoi partition.

III. Algorithm Design & Analysis

Here, we propose and analyze two algorithms suited to the the problem of online estimation and coverage in multi-fidelity settings. The first, Stochastic-sequencing of Multi-fidelity Learning and Coverage (SMLC), is inspired by the centralized server-based algorithm proposed in [11]. The second, Deterministic-sequencing of Multi-fidelity Learning and Coverage (DMLC), is inspired by the Deterministic Sequencing of Learning and Coverage algorithm proposed in [16]. Both algorithms leverage low-fidelity observations collected prior to the start of the algorithm's execution in conjunction with high-fidelity observations collected in real-time by agents to infer a multi-fidelity estimate of ϕ and perform coverage with respect to this estimate. Each gradually shifts emphasis from learning to coverage as the estimate converges to the true sensory function ϕ. Throughout, we refer to the estimate of ϕ at iteration t by $\hat{\phi}^{(t)}$.

A. Stochastic-sequencing of Multi-fidelity Learning and Coverage (SMLC)

Inspired by [11], the SMLC algorithm is characterized by a stochastic decision process governing whether agent i is tasked with *learning* or *coverage* at iteration t. A global multi-fidelity model $\hat{\phi}^{(t)}$ of ϕ is maintained by aggregating low-fidelity observations $(\boldsymbol{X}_\ell, \boldsymbol{y}_\ell)$ with high-fidelity observations $(\boldsymbol{X}_h, \boldsymbol{y}_h)$ on a centralized server. It is assumed the observations $(\boldsymbol{X}_\ell, \boldsymbol{y}_\ell)$ are collected from an auxiliary source prior to the start of the algorithm's execution, while the observations $(\boldsymbol{X}_h, \boldsymbol{y}_h)$ are collected in real-time by agents.

Define $\mathcal{V}_\mathcal{D}^{(t)} = \{v_1^{(t)}, \ldots, v_n^{(t)}\}$ as the Voronoi partition associated with centroid locations $\boldsymbol{c}_i^{(t-1)}$ from the previous

Algorithm 1: Stochastic Multi-Fidelity Learning & Coverage (SMLC)

Input : Low-fidelity observations $(\boldsymbol{X}_\ell, \boldsymbol{y}_\ell)$, initial configuration $\boldsymbol{\eta}^{(0)}$ and strictly increasing decision function $F : [0,1] \to [0,1]$.

Initialize MFGP model $\hat{\phi^{(t)}}$ with low-fidelity data $(\boldsymbol{X}_\ell, \boldsymbol{y}_\ell)$ and initialize a Voronoi partition $\mathcal{V}_\mathcal{D}^{(t)} = \{v_1^{(t)}, \dots, v_N^{(t)}\}$ generated by $\boldsymbol{\eta}^{(0)}$. Compute the maximum posterior variance $M^{(0)}$.

for *iteration* $t = 1, 2, \dots$ **do**

Model and partition update:

Agents update $\hat{\phi}^{(t)}$ with $(\boldsymbol{X}_h, \boldsymbol{y}_h)$ from iteration $t-1$.

Construct Voronoi partition $\mathcal{V}_\mathcal{D}^{(t)}$ from previous centroids $\boldsymbol{c}_i^{(t-1)}$ and estimate $\hat{\phi}^{(t)}$. Compute new centroids $\boldsymbol{c}_i^{(t)}$.

for *agent* $i = 1, 2, \dots, N$ **do**

Stochastic decision:

Compute maximum posterior variance within v_i: $M_{v_i}^{(t)} = \max_{\boldsymbol{x} \in v_i^{(t)}} \text{var}_\phi^{(t)}(\boldsymbol{x})$.

Set $p_i^{(t)} = F(M_{v_i}^{(t)} / M^{(0)})$ and $b_i^{(t)} \sim \text{Bernoulli}(p_i^{(t)})$.

if $b_i^{(t)} == 1$ **then**

Learning step:

Agent i samples ϕ as $y_h = \phi_h(\boldsymbol{x}) + \epsilon_h$ where $\epsilon_h \sim \mathcal{N}(0, \sigma_h^2)$ at the point $\boldsymbol{x}_{M_{v_i}}^{(t)} = \arg\max_{\boldsymbol{x} \in v_i^{(t)}} \text{var}_\phi^{(t)}(\boldsymbol{x})$.

else

Coverage step:

Agent i drives to the centroid $\boldsymbol{c}_i^{(t)}$ of $v_i^{(t)}$.

Algorithm 2: Deterministic Multi-Fidelity Learning & Coverage (DMLC)

Input : Low-fidelity observations $(\boldsymbol{X}_\ell, \boldsymbol{y}_\ell)$, initial configuration $\boldsymbol{\eta}^{(0)}$, $\alpha \in (0,1)$ and $\beta > 1$.

Initialize MFGP model $\hat{\phi}^{(t)}$ with low-fidelity data $(\boldsymbol{X}_\ell, \boldsymbol{y}_\ell)$ and initialize a Voronoi partition $\mathcal{V}_\mathcal{D}^{(t)} = \{v_1^{(t)}, \dots, v_N^{(t)}\}$ generated by $\boldsymbol{\eta}^{(0)}$. Compute the maximum posterior variance $M^{(0)}$.

for *epoch* $e = 1, 2, \dots$ **do**

Learning phase:

A central server virtually samples $\boldsymbol{x}_M^{(t)} = \arg\max_{\boldsymbol{x} \in \mathcal{D}} \text{var}_\phi^{(t)}(\boldsymbol{x})$ using a greedy policy to determine the set of points $\boldsymbol{X}_o^{(e)}$ which must be sampled to reduce $M^{(t)} \leq \alpha^e M^{(0)}$.

Points $\boldsymbol{X}_o^{(e)}$ are grouped by Voronoi cell $v_i^{(t)}$, and TSP tours are computed through each subset $\boldsymbol{X}_o^{(e)} \cap v_i^{(t)}$.

Agents sample points along their TSP tour and update the MFGP $\hat{\phi}$ with observations $(\boldsymbol{X}_h, \boldsymbol{y}_h)$ where $\boldsymbol{y}_h = \phi(\boldsymbol{X}_h) + \epsilon_h$ with $\epsilon_h \sim \mathcal{N}(0, \sigma_h^2)$.

Coverage phase:

for $t_e = 1, 2, \dots, \lceil \beta^e n_{e_0} \rceil$ **do**

Construct Voronoi partition $\mathcal{V}_\mathcal{D}^{(t)}$ from previous centroids $\boldsymbol{c}_i^{(t-1)}$ and estimate $\hat{\phi}^{(t)}$. Compute new centroids $\boldsymbol{c}_i^{(t)}$.

Each agent i drives to the centroid $\boldsymbol{c}_i^{(t)}$ of $v_i^{(t)}$.

iteration, where $\boldsymbol{c}^{(0)} = \boldsymbol{\eta}^{(0)}$. Agents update $\mathcal{V}_\mathcal{D}^{(t)}$ at the start of each iteration t, then each agent stochastically chooses to execute a *learning* step or a *coverage* step. The probability $p_i^{(t)}$ of agent i executing a *learning* step on iteration t is proportional to the maximum posterior variance $M_{v_i}^{(t)} = \max_{\boldsymbol{x} \in v_i^{(t)}} \text{var}_\phi^{(t)}(\boldsymbol{x})$ of the current estimate $\hat{\phi}^{(t)}$ within $v_i^{(t)}$, and the probability that the agent executes a *coverage* step is $1 - p_i^{(t)}$.

On a *learning* step, agent i collects a noisy high-fidelity sample $y = \phi_h(\boldsymbol{x}_i) + \varepsilon_h$ with $\varepsilon_h \sim \mathcal{N}(0, \sigma_h^2)$ at the point $\boldsymbol{x}_{M_{v_i}}^{(t)} = \arg\max_{\boldsymbol{x} \in v_i^{(t)}} \text{var}_\phi^{(t)}(\boldsymbol{x})$ of maximum posterior variance within $v_i^{(t)}$. On a *coverage* step, agent i proceeds to the centroid $\boldsymbol{c}_i^{(t)}$ of its Voronoi cell (3). Before continuing onto the next iteration, the estimate $\hat{\phi}^{(t)}$ is recomputed by incorporating the samples collected by agents which executed a learning step on this iteration. As more samples are collected, the maximum posterior variance $M_{v_i}^{(t)}$ of $\hat{\phi}^{(t)}$ within each cell $v_i^{(t)}$ will decrease. This drives a gradual shift in emphasis from learning to coverage as $\hat{\phi}^{(t)}$ converges to the true sensory function ϕ over the course of the algorithm's execution. A schematic of the SMLC algorithm is presented in Algorithm 1.

B. Deterministic-sequencing of Multi-fidelity Learning and Coverage (DMLC)

The DMLC algorithm, inspired by [16], is characterized by a deterministic sequencing of epochs $e \in \mathbb{N}$ where each epoch consists of a *learning* and a *coverage* phase. Each epoch e lasts for n_e iterations, and successive epochs increase in length such that uncertainty at the end of these epochs reduces exponentially (see Algorithm 2). As before, a global multi-fidelity model $\hat{\phi}^{(t)}$ of ϕ is maintained by aggregating low-fidelity observations $(\boldsymbol{X}_\ell, \boldsymbol{y}_\ell)$ with high-fidelity observations $(\boldsymbol{X}_h, \boldsymbol{y}_h)$ on a centralized server. We maintain the assumption that low-fidelity observations are collected before the algorithm begins and high-fidelity observations are collected in real-time by agents, and again assume agents operate within the cells $v_i^{(t)}$ of a Voronoi partition $\mathcal{V}_\mathcal{D}^{(t)}$.

Two hyperparameters govern the progression of DMLC, namely α and β. The hyperparameter $\alpha \in (0,1)$ represents the factor by which maximum posterior variance $M^{(t)} = \max_{\boldsymbol{x} \in \mathcal{D}} \text{var}_\phi^{(t)}(\boldsymbol{x})$ is reduced in epoch e, while the hyperparameter $\beta > 1$ represents the factor by which epoch length increases. DMLC begins epoch e with a *learning* phase in which a sufficient number of observations $(\boldsymbol{X}_h, \boldsymbol{y}_h)$ are collected in order to reduce $M^{(t)}$ by a factor of α, then proceeds to execute a *coverage* phase in which agents are driven by Lloyd iteration (4).

Because the posterior variance $\text{var}_\phi^{(t)}(\boldsymbol{x})$ at each point $\boldsymbol{x} \in \mathcal{D}$ is independent of the value of $\hat{\phi}^{(t)}$ under a GP model [23], the entire set of points $\boldsymbol{X}_o^{(e)}$ which must be observed to reduce $M^{(t)}$ by a factor of α in epoch e may be computed before any observations are actually collected. DMLC takes advantage of this fact, and determines the set $\boldsymbol{X}_o^{(e)}$ at the start of epoch e by assuming points of maximum posterior variance $\boldsymbol{x}_{M_{v_i}}^{(t)} = \arg\max_{\boldsymbol{x} \in v_i} \text{var}_\phi(\boldsymbol{x})$ are (virtually) sampled, (virtually) adding such points to

$\boldsymbol{X}_o^{(e)}$, and (virtually) recomputing the posterior variance with such points taken into account. This process is carried out proactively before the learning phase begins.

Once the set of points $\boldsymbol{X}_o^{(e)}$ to be observed in epoch e has been determined, the learning phase begins by grouping the points $\boldsymbol{x} \in \boldsymbol{X}_o^{(e)}$ by the Voronoi cell v_i in which they fall, and assigning such $\boldsymbol{x} \in \boldsymbol{X}_o^{(e)} \cap v_i$ to be sampled by agent i. Next, DMLC computes near-optimal Traveling Salesman Problem (TSP) tours through these points, and directs agents to sample the points on their respective tour. As opposed to naïve greedy sampling algorithms which reactively drive agents to points $\boldsymbol{x}_{M_{v_i}}^{(t)}$ as data is collected, this TSP-inspired approach is more efficient in terms of travel time and energy expenditure. Noisy, high-fidelity samples are collected at all points in $\boldsymbol{X}_o^{(e)}$ and aggregated into the observation set $(\boldsymbol{X}_h, \boldsymbol{y}_h)$, and the learning phase of DMLC concludes.

Finally, DMLC proceeds to perform a *coverage* phase by executing Lloyd's algorithm (4), sending all agents to the centroid $\boldsymbol{c}_i$ of their respective Voronoi cell (3). Epoch length n_e is updated with $n_{e+1} = \beta n_e$, and the algorithm repeats. This exponential growth in epoch length leads agents to gradually shift their emphasis from learning to coverage in a manner similar to that of SMLC. A schematic of the DMLC algorithm is presented in Algorithm 2.

It is worth comparing SMLC and DMLC at a high level before proceeding. DMLC offers a strict bound on the maximum posterior variance $M^{(t)}$ by construction, and tends to minimize the distance agents travel over the course of execution by determining sample points and computing TSP tours in advance. On the other hand, SMLC offers a smoother transition from learning to coverage by decoupling the behavior of agents and allowing some to perform *learning* steps while others perform *coverage* steps. Both algorithms may be implemented in a distributed manner by leveraging gossip-based strategies [24], as proposed in the original works [11] and [16]. In addition, both algorithms can be adapted to use a single-fidelity GP by combining samples $(\boldsymbol{X}_\ell, \boldsymbol{y}_\ell)$ and $(\boldsymbol{X}_h, \boldsymbol{y}_h)$ into a single dataset $(\boldsymbol{X}, \boldsymbol{y})$. Although this largely eliminates their novelty, such single-fidelity adaptations are useful for comparison purposes and serve as a baseline in the simulations presented in Section IV.

C. Analysis of SMLC and DMLC

A key strength of the original algorithms proposed in [11] and [16] are the convergence guarantees they offer. Specifically, Proposition 1 of [11] guarantees that the application of Lloyd's algorithm (4) to the estimate $\hat{\phi}^{(t)}$ will asymptotically mimic the evolution of Lloyd's algorithm applied to the ground truth ϕ if $\hat{\phi}^{(t)}$ converges in probability to the true sensory function ϕ. We adapt Proposition 2 of [11] to show that the estimate $\hat{\phi}^{(t)}$ will indeed converge in probability ϕ under the SMLC and DMLC algorithms, thereby implying that Proposition 1 in [11] also holds for SMLC and DMLC. These results are formally presented in the following propositions.

Let $\hat{\boldsymbol{c}}_i^{(t)}$ denote the centroid (3) of the Voronoi cell assigned to agent i at iteration t, computed with respect to the estimated sensory function $\hat{\phi}^{(t)}$. Similarly, let $\boldsymbol{c}_i^{(t)}$ denote the true centroid of cell i at iteration t. The following result (Proposition 1 of [11]) asserts that the evolution of $\hat{\boldsymbol{c}}_i^{(t)}$ and $\boldsymbol{c}_i^{(t)}$ will remain arbitrarily close with high probability for an arbitrary (but finite) number of iterations.

*Proposition 1 (**Lloyd Equivalence, Proposition 1, [11]**):* Assume $\hat{\phi}^{(t)}$ converges in probability to ϕ. Choose any $\delta \in (0,1)$, $\varepsilon > 0$, and integer N. Suppose the centroids $\hat{\boldsymbol{c}}_i^{(t)}$ and $\boldsymbol{c}_i^{(t)}$ are updated according to the standard Lloyd algorithm (4). Then there exists an iteration t_0 such that

$$P\left(\left\|\hat{\boldsymbol{c}}_i^{(t_0+t)} - \boldsymbol{c}_i^{(t_0+t)}\right\| \leq \varepsilon\right) \geq 1-\delta \tag{10}$$

for all iterations $t = 0, \ldots, N$ and cells i when the estimated and true centroid begin in the same location: $\hat{\boldsymbol{c}}_i^{(t_0)} = \boldsymbol{c}_i^{(t_0)}$.

Now, we show both SMLC and DMLC guarantee that $\hat{\phi}^{(t)}$ converges in probability to ϕ, so that Proposition 1 holds. Let $M^{(t)} = \max_{\boldsymbol{x}\in\mathcal{D}} \mathrm{var}_\phi^{(t)}(\boldsymbol{x})$ denote the maximum posterior variance of the estimate $\phi^{(t)}$ at iteration t. Further, let $\boldsymbol{x}_M^{(t)} = \arg\max_{\boldsymbol{x}\in\mathcal{D}} \mathrm{var}_\phi^{(t)}(\boldsymbol{x})$ be the point at which $M^{(t)}$ is achieved.

*Proposition 2 (**Convergence of SMLC Estimate**):* Consider the SMLC algorithm presented in Algorithm 1 with the multi-fidelity GP model (5). Let $F : [0,1] \to [0,1]$ be a continuous and strictly increasing function of $M^{(t)}$. Then $\hat{\phi}^{(t)}$ converges in probability to the true function ϕ.

Proof: We provide a sketch of the proof. The structure of the SMLC algorithm is identical to that of the server-based (SB) algorithm proposed in [11], differing only in its use of a MFGP. Yet, $\hat{\phi}^{(t)}$ is itself a GP with composite covariance function $k(\boldsymbol{x}, \boldsymbol{x})$ as shown in (8). Observations from lower fidelity levels makes $\hat{\phi}^{(t)}$ converge faster to ϕ. Thus, the result follows by Proposition 2 provided in [11]. ■

*Proposition 3 (**Convergence of DMLC Estimate**):* Consider the DMLC algorithm presented in Algorithm 2 with the multi-fidelity GP model (5). Let $\alpha \in (0,1)$ denote the factor by which maximum posterior variance $M^{(t)}$ is reduced in each epoch. Then $\hat{\phi}^{(t)}$ converges in probability to the true function.

Proof: Let $\bar{\phi}(\boldsymbol{x}) \sim GP(\bar{\mu}(\boldsymbol{x}), \bar{k}(\boldsymbol{x}, \boldsymbol{x}'))$ be a GP defined on $\bar{\mathcal{D}} \subseteq \mathcal{D}$, where covariance function $\bar{k}(\boldsymbol{x}, \boldsymbol{x}')$ is continuous and $\bar{k}(\boldsymbol{x}, \boldsymbol{x}) \leq \lambda, \forall \boldsymbol{x} \in \bar{\mathcal{D}}$. Let σ^2 be the variance of additive Gaussian sampling noise. Now, we show the greedy sampling strategy reduces the maximum variance below threshold ε in finite iterations for any fixed ε. Note that for every $\varepsilon > 0$, there exist γ, ν and n that satisfy

$$\lambda - (\lambda-\gamma)^2 / \left(\lambda + \nu + \frac{\sigma^2}{n}\right) \leq \varepsilon.$$

Since $\bar{k}(\boldsymbol{x}, \boldsymbol{x}')$ is continuous, there exists a finite partition $P = \{p_1, \ldots, p_m\}$ of $\bar{\mathcal{D}}$, with m large enough, such that for any $p_i \in P$ and for any pair of points $\boldsymbol{x}, \boldsymbol{x}' \in p_i$,

$$\left|\bar{k}(\boldsymbol{x}, \boldsymbol{x}) - \bar{k}(\boldsymbol{x}, \boldsymbol{x}')\right| \leq \gamma, \quad \left|\bar{k}(\boldsymbol{x}, \boldsymbol{x}) - \bar{k}(\boldsymbol{x}', \boldsymbol{x}')\right| \leq \nu.$$

After $nm+1$ sampling rounds, there exists at least one cell $p_i \in P$ that is selected $n_i \geq (n+1)$ times. Let $X \in \mathbb{R}^{2\times n}$ be the matrix of first n sampling locations within p_i and $\boldsymbol{y} \in \mathbb{R}^n$

be the corresponding sampling results. Then, for any $\boldsymbol{x} \in p_i$, $\max_{\boldsymbol{x}' \in p_i} \bar{k}(\boldsymbol{x}', \boldsymbol{x}') \leq \bar{k}(\boldsymbol{x}, \boldsymbol{x}) + \nu$. Let $\bar{K}(X, X) \in \mathbb{R}^{n \times n}$ be the covariance matrix with entries $\{\bar{k}(\boldsymbol{x}', \boldsymbol{x}'')\}_{\boldsymbol{x}', \boldsymbol{x}'' \in X}$ and $\bar{K}(X, \boldsymbol{x}) = \bar{K}^\top(\boldsymbol{x}, X) \in \mathbb{R}^{n \times n}$ be the vector with entries $\{\bar{k}(\boldsymbol{x}, \boldsymbol{x}')\}_{\boldsymbol{x}' \in X}$. Using the Gershgorin circle theorem [25], the spectral radius of symmetric matrix $\bar{K}(X, X) + \sigma^2 I$ is no greater than $n(\bar{k}(\boldsymbol{x}, \boldsymbol{x}) + \nu) + \sigma^2$. Thus, for every $\boldsymbol{x} \in p_i$

$$
\begin{aligned}
&\mathrm{var}_{\bar{\phi}}(\boldsymbol{x} | X, \boldsymbol{y}) \\
&= \bar{k}(\boldsymbol{x}, \boldsymbol{x}) - \bar{K}(\boldsymbol{x}, X) \left(\bar{K}(X, X) + \sigma^2 I \right)^{-1} \bar{K}(X, \boldsymbol{x}) \\
&\leq \bar{k}(\boldsymbol{x}, \boldsymbol{x}) - \frac{\left\| \bar{K}(X, \boldsymbol{x}) \right\|_2^2}{n(\bar{k}(\boldsymbol{x}, \boldsymbol{x}) + \nu) + \sigma^2} \\
&\leq \bar{k}(\boldsymbol{x}, \boldsymbol{x}) - \frac{(\bar{k}(\boldsymbol{x}, \boldsymbol{x}) - \gamma)^2}{\bar{k}(\boldsymbol{x}, \boldsymbol{x}) + \nu + \frac{\sigma^2}{n}} \leq \lambda - \frac{(\lambda - \gamma)^2}{\lambda + \nu + \frac{\sigma^2}{n}} \leq \varepsilon,
\end{aligned}
$$

where we use the fact $x - (x - \gamma)^2 / (x + \nu + \frac{\sigma^2}{n})$ increases with x for $x > 0$. Since the variance at every point in p_i is smaller than ε after n samples and p_i is selected $n_i \geq (n+1)$ times, the variance at every point $\boldsymbol{x} \in \mathcal{D}$ must be smaller than ε when p_i is selected $(n+1)$-th time by the greedy policy, i.e., after $nm + 1$ overall samples have been collected.

This shows each learning step in DMLC can be finished in finite iterations. Thus, for and ε and δ, there is a finite t' for which $M^{(t)} \leq \delta \varepsilon^2$ holds for all $t > t'$. Now, by the Chebyshev inequality, we have $P(|\hat{\phi}^{(t)}(\boldsymbol{x}) - \bar{\phi}(\boldsymbol{x})| \geq \varepsilon) \leq \mathrm{var}_{\phi}^{(t)}(\boldsymbol{x}) / \varepsilon^2 \leq \delta$ at any point $\boldsymbol{x} \in \mathcal{D}$ for all $t > t'$, which concludes the proof. ■

IV. Simulations

Multi-fidelity approaches to online estimation and coverage are as promising in practice as they are in theory. Given data from heterogeneous sources, simulations show that multi-fidelity implementations of SMLC and DMLC tend to outperform single-fidelity implementations. In particular, multi-fidelity implementations of SMLC and DMLC incur lower instantaneous coverage regret (9) and lower mean squared error $||\hat{\phi}(\boldsymbol{X}^*) - \phi(\boldsymbol{X}^*)||^2 \ / \ |\boldsymbol{X}^*|$ in estimating and covering ϕ, where $\boldsymbol{X}^* \subset \mathcal{D}$ is finite with cardinality $|\boldsymbol{X}^*|$.

As presented in Section III, the SMLC and DMLC algorithms are assumed to leverage a multi-fidelity GP learning model by default. However, one may replace this multi-fidelity GP with a traditional single-fidelity GP, changing the learning dynamics while maintaining the fundamental structure of each algorithm. Thus we refer to versions of SMLC and DMLC which use multi-fidelity GPs as "multi-fidelity implementations," and refer to those which use single-fidelity GPs as "single-fidelity implementations." We emphasize that the key novelty of SMLC and DMLC is their use of multi-fidelity models—we consider implementations which use single-fidelity models only as a baseline.

To empirically compare the multi-fidelity implementations of SMLC and DMLC with single-fidelity implementations, we conducted a series of simulations over a 21×21 point discretization of the unit square $\mathcal{D} = [0, 1]^2$ with four agents. For simplicity, we limited our consideration to the existence of two fidelity levels $f \in \{h, \ell\}$ such that the multi-fidelity

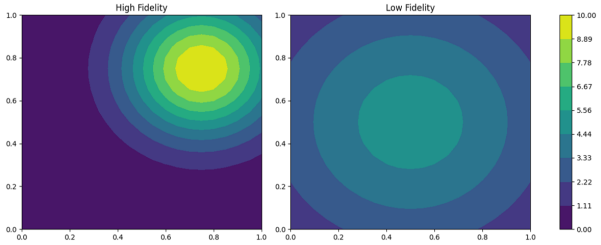

Fig. 2: Sensory functions ϕ_h (left) and ϕ_ℓ (right) defined in (11) and used in simulations. Note that ϕ_h and ϕ_ℓ are correlated such that low-fidelity samples provide insight into ϕ_h.

GP model proposed in Section II reduces to $\phi_h = \rho \phi_\ell + \delta_h$ and $\phi_\ell = \delta_\ell$. We define ϕ_h and ϕ_ℓ as

$$
\phi_f = v_f^2 \exp\left(- \left\| \boldsymbol{x} - \boldsymbol{c}_f \right\|^2 / 2 l_f^2 \right), \quad f \in \{h, \ell\}, \tag{11}
$$

with $v_\ell = \sqrt{5}$, $l_\ell = \sqrt{0.2}$, $\boldsymbol{c}_\ell = [0.5, 0.5]^\top$ and $v_h = \sqrt{10}$, $l_h = \sqrt{0.05}$, $\boldsymbol{c}_h = [0.75, 0.75]^\top$ as shown in Figure 2. Importantly, ϕ_ℓ and ϕ_h as defined in (11) are correlated such that access to low-fidelity samples $(\boldsymbol{X}_\ell, \boldsymbol{y}_\ell)$ with $\boldsymbol{y}_\ell = \phi_\ell(\boldsymbol{X}_\ell) + \varepsilon_\ell$, $\varepsilon_\ell \sim \mathcal{N}(0, \sigma_\ell^2)$ provides insight into the behavior of ϕ_h, despite the fact that ϕ_ℓ itself is biased from the ground truth. Such sensory functions may occur when low-fidelity data identifies a broad region of interest and the event is approximated by a Gaussian centered at the center of this region, while high-fidelity input is able to better localize the region of interest.

Twenty-five low-fidelity samples at the points $\boldsymbol{X}_\ell = \{[0.25i, 0.25j]^\top \in \mathcal{D} \mid 0 \leq i, j \leq 4\}$ drawn from ϕ_ℓ with Gaussian noise $\sigma_\ell^2 = 1$ were provided to initialize the learning model of each algorithm. Thereafter, all samples $(\boldsymbol{X}_h, \boldsymbol{y}_h)$ collected by agents were drawn from ϕ_h with Gaussian noise $\sigma_h^2 = 1$. Because the single-fidelity implementations of SMLC and DMLC cannot distinguish fidelity levels, they combine all observations $(\boldsymbol{X}_\ell, \boldsymbol{y}_\ell)$ and $(\boldsymbol{X}_h, \boldsymbol{y}_h)$ into a single dataset $(\boldsymbol{X}, \boldsymbol{y})$ throughout the learning process. In contrast, the multi-fidelity implementations of SMLC and DMLC maintain separate datasets.

We simulated the standard, non-adaptive coverage control algorithm presented in [2] which assumes perfect knowledge of ϕ_h as a baseline to compare against. Single and multi-fidelity GP models were implemented in Python by adapting existing open-source code [26], and GP hyperparameters were fit to maximum likelihood estimates given 100 training samples from (11) using standard optimization techniques. Other simulation parameters used throughout are summarized in Table I. Videos of our simulations, along with the code used to conduct them, are available via GitHub [27].

Key results of our simulations are shown in Figure 3. In particular, panel (a) compares the instantaneous coverage regret (9) incurred by SMLC and DMLC using single- and multi-fidelity learning models, and shows that the multi-fidelity implementation of both algorithms outperforms the single-fidelity implementation when provided low-fidelity data $(\boldsymbol{X}_\ell, \boldsymbol{y}_\ell)$ prior to execution. This is due to the fact the multi-fidelity model is able to structurally distinguish

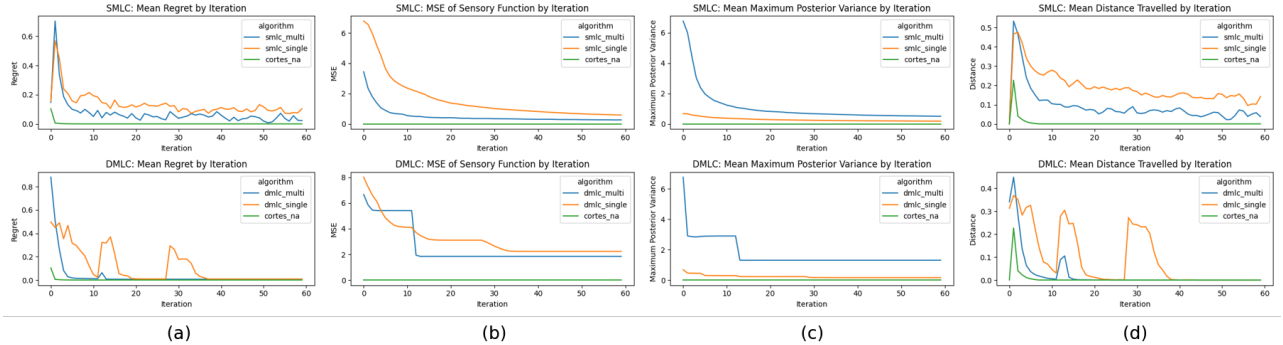

Fig. 3: Simulation results averaged over 50 runs per algorithm-fidelity pair. Blue lines correspond to multi-fidelity implementations, orange lines correspond to single-fidelity implementations and green lines correspond to the baseline from [2] which assumes perfect knowledge of ϕ_h. Panel (a) shows instantaneous coverage regret (9); Panel (b) shows mean squared error of the estimate $\hat{\phi}^{(t)}$ with respect to ϕ; Panel (c) shows maximum posterior variance $M^{(t)}$; Panel (d) shows distance travelled. Simulation parameters are presented in Table I. Sensory function ϕ is defined in (11) and visualized in Figure 2. Code and videos are available online [27].

TABLE I: Simulation parameters. Code and videos available online [27].

Parameter	**Value**
Number of agents	4
Number of iterations per simulation	60
Number of simulations per algorithm	50
SMLC decision function F	$F(x) = x$
DMLC reduction parameter α	$\sqrt{2}$
DMLC epoch length multiplier β	2
DMLC epoch lengths	$[4, 8, 16, 32]$
Algorithms simulated	Cortes [2], SMLC, DMLC

between low-fidelity and high-fidelity data, and estimation of model hyperparameters ensures that (in)consistency between these data are appropriately captured and incorporated. The single-fidelity model does not provide this flexibility.

Panel (b) compares the mean squared error $||\hat{\phi}(\boldsymbol{X}^*) - \phi(\boldsymbol{X}^*)||^2 \;/\; |\boldsymbol{X}^*|$ of the estimate $\hat{\phi}^{(t)}$, affirming that multi-fidelity methods learn a more accurate representation of ϕ than single-fidelity methods when provided low-fidelity data as they are designed to do. Panel (c) compares the evolution of maximum posterior variance $M^{(t)} = \max_{\boldsymbol{x}\in\mathcal{D}} \text{var}_{\phi}^{(t)}(\boldsymbol{x})$, and highlights another key advantage offered by the multi-fidelity implementation of each algorithm: more nuanced quantification of uncertainty. Because the single-fidelity implementations cannot distinguish between observations $(\boldsymbol{X}_\ell, \boldsymbol{y}_\ell)$ and $(\boldsymbol{X}_h, \boldsymbol{y}_h)$, the estimate $\hat{\phi}^{(t)}$ is overconfident and does not account for potential bias introduced by low-fidelity observations. Finally, panel (d) compares the mean distance travelled by each agent over the course of execution. Evidently, the single-fidelity implementation of each algorithm does not converge as smoothly due to the initial bias introduced by low-fidelity observations, leading to excessive motion. It is also worth noting that panel (d) confirms agents executing DMLC travel less distance on average than agents executing SMLC, as discussed in Section III.

V. Conclusion

Heterogeneous multi-robot sensing systems offer a performance advantage over homogeneous systems due to their ability to learn more accurate representations of physical processes by fusing information from multiple distinct modalities. However, the method used to combine heterogeneous data plays a crucial role in system performance and merits principled consideration. In this work, we used multi-fidelity Gaussian Processes (GPs) to combine heterogeneous data of different *fidelities* collected by a heterogeneous multi-robot sensing system. We applied this approach to the task of online estimation and coverage in which an unknown sensory function ϕ must be learned and covered by agents, and illustrated scenarios in which single-fidelity approaches fall short. We proposed two novel adaptive coverage algorithms which leverage the multi-fidelity GP framework—namely Stochastic-sequencing of Multi-fidelity Learning and Coverage (SMLC) and Deterministic-sequencing of Multi-fidelity Learning and Coverage (DMLC)—and prove the asymptotic convergence of both algorithms. We demonstrate the empirical efficacy of SMLC and DMLC through numerical simulations, and provide the code used to conduct them via GitHub [27].

References

[1] G. Hallegraeff, "Harmful algal blooms: A global overview," *Manual on Harmful Marine Microalgae*, vol. 33, pp. 1–22, 2003.

[2] J. Cortés, S. Martínez, T. Karataş, and F. Bullo, "Coverage control for mobile sensing networks," *IEEE Transactions on Robotics and Automation*, vol. 20, no. 2, pp. 243–255, 2004.

[3] I. I. Hussein, D. M. Stipanović, and Y. Wang, "Reliable coverage control using heterogeneous vehicles," in *Proceedings of the IEEE Conference on Decision and Control*, 2007, pp. 6142–6147.

[4] L. C. Pimenta, V. Kumar, R. C. Mesquita, and G. A. Pereira, "Sensing and coverage for a network of heterogeneous robots," in *Proceedings of the IEEE Conference on Decision and Control*. IEEE, 2008, pp. 3947–3952.

[5] Y. Kantaros, M. Thanou, and A. Tzes, "Distributed coverage control for concave areas by a heterogeneous robot–swarm with visibility sensing constraints," *Automatica*, vol. 53, pp. 195 – 207, 2015.

[6] O. Arslan and D. E. Koditschek, "Voronoi-based coverage control of heterogeneous disk-shaped robots," in *Proceedings of the IEEE International Conference on Robotics and Automation*. IEEE, 2016, pp. 4259–4266.

[7] A. Pierson, L. C. Figueiredo, L. C. Pimenta, and M. Schwager, "Adapting to sensing and actuation variations in multi-robot coverage," *The International Journal of Robotics Research*, vol. 36, no. 3, pp. 337–354, 2017.

[8] M. Santos, Y. Diaz-Mercado, and M. Egerstedt, "Coverage control for multi-robot teams with heterogeneous sensing capabilities," *IEEE Robotics and Automation Letters*, vol. 3, no. 2, pp. 5313–5319, 2018.

[9] J. Choi, J. Lee, and S. Oh, "Swarm intelligence for achieving the global maximum using spatio-temporal Gaussian processes," in *Proceedings of the American Control Conference*, 2008, pp. 135–140.

[10] M. Schwager, D. Rus, and J. J. Slotine, "Decentralized, adaptive coverage control for networked robots," *International Journal of Robotics Research*, vol. 28, no. 3, pp. 357–375, 2009.

[11] M. Todescato, A. Carron, R. Carli, G. Pillonetto, and L. Schenato, "Multi-robots Gaussian estimation and coverage control: From client–server to peer-to-peer architectures," *Automatica*, vol. 80, pp. 284–294, 2017.

[12] M. Schwager, M. P. Vitus, S. Powers, D. Rus, and C. J. Tomlin, "Robust adaptive coverage control for robotic sensor networks," *IEEE Transactions on Control of Network Systems*, vol. 4, no. 3, pp. 462–476, 2017.

[13] W. Luo and K. Sycara, "Adaptive Sampling and Online Learning in Multi-Robot Sensor Coverage with Mixture of Gaussian Processes," in *Proceedings of the IEEE International Conference on Robotics and Automation*. IEEE, 2018, pp. 6359–6364.

[14] W. Luo, C. Nam, G. Kantor, and K. Sycara, "Distributed environmental modeling and adaptive sampling for multi-robot sensor coverage," in *Proceedings of the International Joint Conference on Autonomous Agents and Multiagent Systems, AAMAS*, 2019, pp. 1488–1496.

[15] A. Benevento, M. Santos, G. Notarstefano, K. Paynabar, M. Bloch, and M. Egerstedt, "Multi-robot coordination for estimation and coverage of unknown spatial fields," in *Proceedings of the IEEE International Conference on Robotics and Automation*. IEEE, 2020, pp. 7740–7746.

[16] L. Wei, A. McDonald, and V. Srivastava, "Regret analysis of distributed gaussian process estimation and coverage," in *Proceedings of the IEEE International Conference on Robotics and Automation*. Under Review. Xi'an, China: IEEE, 2021, arXiv preprint: https://arxiv.org/abs/2101.04306.

[17] A. Sadeghi and S. L. Smith, "Coverage control for multiple event types with heterogeneous robots," in *Proceedings of the IEEE International Conference on Robotics and Automation*. IEEE, 2019, pp. 3377–3383.

[18] P. Reverdy, V. Srivastava, and N. E. Leonard, "Modeling human decision making in generalized Gaussian multiarmed bandits," *Proceedings of the IEEE*, vol. 102, no. 4, pp. 544–571, 2014.

[19] L. Wei, X. Tan, and V. Srivastava, "Expedited multi-target search with guaranteed performance via multi-fidelity Gaussian Processes," in *IEEE/RSJ International Conference on Intelligent Robots and Systems*, Las Vegas, NV (Virtual), Oct. 2020, pp. 7095–7100.

[20] A. O. Hero and D. Cochran, "Sensor management: Past, present, and future," *IEEE Sensors Journal*, vol. 11, no. 12, pp. 3064–3075, 2011.

[21] S. P. Lloyd, "Least Squares Quantization in PCM," *IEEE Transactions on Information Theory*, vol. 28, no. 2, pp. 129–137, 1982.

[22] M. Kennedy and A. O'Hagan, "Predicting the output from a complex computer code when fast approximations are available," *Biometrika*, vol. 87, no. 1, pp. 1–13, 2000.

[23] C. E. Rasmussen and C. K. I. Williams, *Gaussian Processes for Machine Learning*. The MIT Press, 2006.

[24] J. W. Durham, R. Carli, P. Frasca, and F. Bullo, "Discrete partitioning and coverage control for gossiping robots," *IEEE Transactions on Robotics*, vol. 28, no. 2, pp. 364–378, 2012.

[25] R. A. Horn and C. R. Johnson, *Matrix Analysis*. Cambridge University Press, 2012.

[26] P. Perdikaris. GP Tutorial: A hands-on tutorial on supervised learning with Gaussian Processes. [Online]. Available: https://github.com/paraklas/GPTutorial

[27] A. McDonald. Multi-fidelity Learning + Coverage: A repository of multifidelity learning + coverage algorithms. [Online]. Available: https://github.com/andrewmcdonald27/multifidelity-learning-coverage